Next Energy 11 (2026) 100602

Contents lists available at ScienceDirect

Next Energy

journal homepage: www.sciencedirect.com/journal/next-energy

Research article

ANFIS-based intelligent control for capacitor voltage stabilization and harmonic mitigation in multilevel active power filters

Syed Zaki ul Hasan Naqvi[a], Yap Hoon[a,*], KuewWai Chew[a], Mohd Amran Mohd Radzi[b]

[a] Lee Kong Chian Faculty of Engineering and Science, Universiti Tunku Abdul Rahman, Kajang, Selangor 43000, Malaysia
[b] Department of Electrical and Electronic Engineering, Faculty of Engineering, Universiti Putra Malaysia, Serdang, Selangor 43400, Malaysia

ARTICLE INFO

Keywords:
Voltage balancing
Dual frequency modulation PWM (DFMPWM)
Active harmonic filter
Uniform switching pattern
Power quality

ABSTRACT

The issue of harmonics in power systems has grown increasingly significant because of the extensive utilization on nonlinear loads, leading to voltage distortion and degradation of power quality. To address these problems, a single-phase shunt-active power filter utilizing a 5-level Cascaded H-Bridge (CHB) inverter is developed, as it provides notable benefits such as modularity, flexibility, and component reduction. However, the CHB inverter encounters voltage imbalance issues across its DC-link capacitors due to uneven switching operations and variations in charging and discharging rates, which negatively affect system efficiency. To mitigate these problems, an Adaptive Neuro-Fuzzy Inference System (ANFIS) control strategy is utilized to ensure the stability of voltages among H-bridge modules and enhance the system's dynamic performance. Furthermore, a dual-frequency multicarrier pulse width modulation (DFMPWM) technique is integrated to distribute the switching pattern evenly across each H-bridge module to improve voltage symmetry. With the combined ANFIS–DFMPWM approach, the proposed system achieves significant harmonic reduction, maintaining total harmonic distortion well below the IEEE-519 standard limit, while improving the power factor (P_f) close to unity and minimizing the angle difference between the supply voltages by the source and the resulting current, thereby enhancing overall power quality.

1. Introduction

In the modern era, the proliferation of power electronic converters in industrial and commercial applications has led to increased interest in multilevel inverters (MLIs) for active power filtering (APF). MLIs are preferred because they can generate superior output waveforms, reduce electromagnetic interference, and switching losses relative to traditional 2-level inverters [1]. Nonetheless, a common issue in MLI operation is the unequal voltage distribution within the DC-link capacitor. Voltage unbalance not only degrades output waveform quality but also increases device stress and decreases system reliability, thereby undermining the effectiveness of MLIs in performing APF [2].

Meanwhile, the various MLI configurations, the most commonly used topologies are the Cascaded H-Bridge (CHB), neutral point clamped, and flying capacitor inverters [3–5]. All techniques have their own strength and weaknesses, which are discussed in detail in Refs. [6,7]. In comparison, the CHB inverter has a more efficient response than other 2 MLI topologies and does not require any clamping elements like diodes, capacitors, and has a smaller number of components [8,9].

In contrast with advantages, when required to generate a higher number of voltage steps, the CHB inverter topology suffers from voltage imbalance issues because of series-connected H-bridge modules. This is due to the fact that producing more output voltage steps requires the use of additional series-connected H-bridge modules. Additionally, the higher the quantity of H-bridge modules, the more switches are required, which increases the overall intricacy of the system [10,11].

Meanwhile, the most suitable algorithm for handling a higher number of switches is multicarrier sinusoidal pulse width modulation (PWM), which includes 2 types: level-shifted PWM (LSPWM) and phase-shifted PWM (PSPWM), classified according to the arrangement of the carrier signals [9,12,13]. For CHB inverters, PSPWM is typically preferred because it provides effective harmonic reduction and ensures efficient power distribution among the H-bridge cells [14]. Meanwhile, LSPWM, also known as Phase Disposition PWM (PDPWM), operates by amplitude shifting among multiple carrier signals and is regarded as a more efficient method than PSPWM for reducing harmonics. In case of CHB topology, LSPWM is generally less preferred because the even distribution among the H-bridge modules is a big problem [12,14].

* Corresponding author.
E-mail address: hoonyap@utar.edu.my (Y. Hoon).

https://doi.org/10.1016/j.nxener.2026.100602
Received 17 December 2025; Received in revised form 23 February 2026; Accepted 12 March 2026

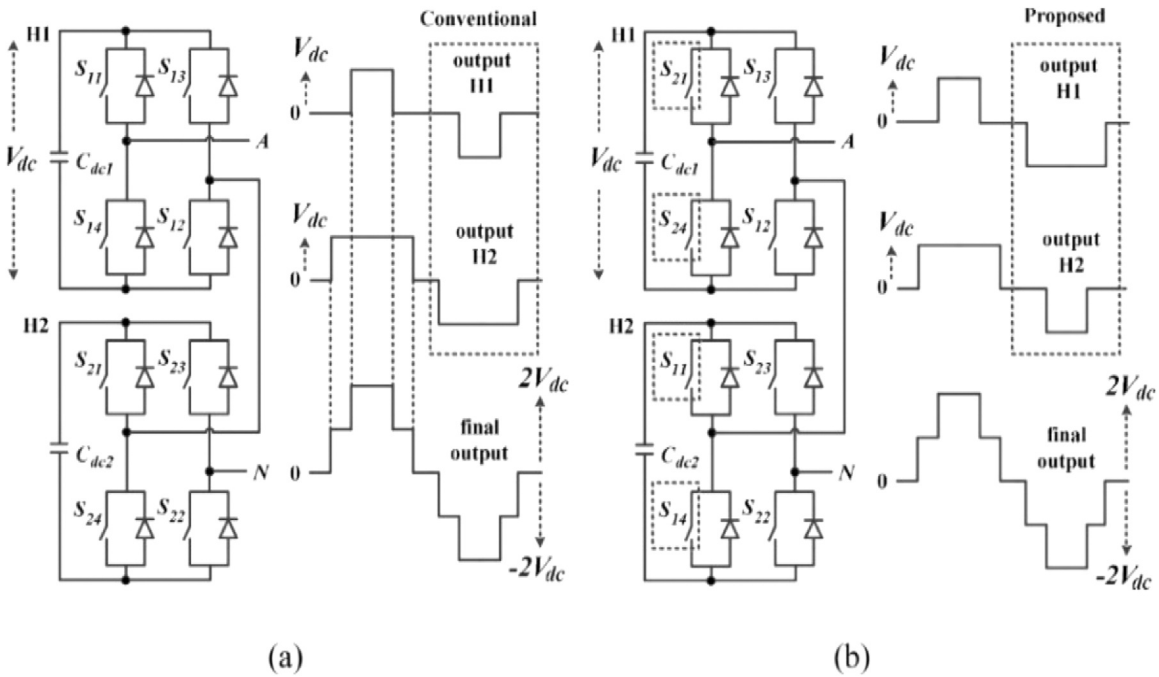

Fig. 1. Configuration of 5-level cascaded H-bridge inverter: (a) conventional setting (b) DFMPWM.

Despite the advantages, various LSPWM-based topologies have been introduced to enhance performance, techniques such as phase-opposed disposition modulation, alternating phase-opposition modulation, and rotating carrier modulation are employed to minimize uneven switching stress on Insulated Gate Bipolar Transistors (IGBTs). These LSPWM variants are implemented in the fundamental operation of the CHB inverter, but still face limitations in managing the complex control of Multilevel Inverter Active Power Filter (MI-APF) systems due to existing harmonics.

To mitigate this problem, Fig. 1 shows another advanced method of LSPWM, proposed in [15] to control the operation of the CHB inverter, and is not widely used in other algorithms, namely dual frequency multicarrier PWM (DFMPWM). As shown in Fig. 1(b), where the pattern of evenly distributed switching signals is proposed, which is integrated in this project to monitor the balancing of the voltages within the dc link capacitor on each H-bridge module.

As shown in Fig. 1, the 5-level CHB inverter consists of 2 H-bridge modules connected in series, each comprising 4 switches. It is vital to preserve uniform voltage across each capacitor. To maintain this, traditional control methods such as Proportional Integral (PI) controllers are commonly employed because of their straightforwardness and ease of implementation, but they often struggle to maintain DC-link voltage balance under varying load and supply conditions. PI controllers require precise tuning and depend on accurate system models, and their fixed gains limit their ability to adapt to nonlinear or uncertain environments [9].

Among these approaches, the Adaptive Neuro-Fuzzy Inference System (ANFIS), a neural network-based adaptive controller, has emerged as a promising technique. ANFIS uses data-driven learning to capture the nonlinear dynamics of MLIs, enabling it to respond effectively to parameter variations and load disturbances. Compared to PI controllers, ANFIS can achieve faster dynamic response, lower steady state error, and more stable capacitor voltage regulation under changing conditions [16]. In the context of APF, applying ANFIS-based voltage balancing control can enhance the harmonic compensation performance of MLIs while maintaining stable capacitor voltages, even under rapidly changing load profiles [17]. Consequently, the adoption of ANFIS for voltage unbalance mitigation directly addresses the current industrial need for reliable, adaptive control solutions in high-performance power electronic systems.

In recent years, the power electronics domain has witnessed a pervasive adoption of artificial intelligence (AI)-based techniques, particularly the ANFIS technique. This surge in popularity can be attributed to the notable performance of ANFIS in effectively handling serious load disturbances and nonlinear loads. Considering these aspects, the integration of ANFIS-based control techniques for voltage balancing offers an effective solution to address voltage imbalance issues and improve the overall efficiency of MI-APF. The aim of this research is to develop an ANFIS-driven voltage balancing algorithm combined with a DFMPWM switching scheme, leveraging AI to enhance MI-APF performance and ensure better power quality within distributed generation systems [16].

The rest of the paper is organized as follows. Section 2 presents the overall control structure of the single-phase shunt-active power filter (SAPF) along with the corresponding power circuit. Section 3 discusses the limitations of the existing method, provides an overview of the DFMPWM technique, and explains the working principle of the proposed ANFIS-based voltage balancing algorithm. Section 4 evaluates the performance of the overall framework and validates the effectiveness of the proposed approach. Finally, Section 5 summarizes the key findings and contributions of the study.

2. Control structure of SAPF inverter

The SAPF inverter's control methodology, depicted in Fig. 2, gives an overview of this project. The harmonics are generated by a rectifier circuit supplying either a capacitive or an inductive load [18,19]. Typically, a 5-level CHB inverter contains 2 H-bridge modules connected in series with 4 switches in each module. In operation, the I_L load current contains both harmonic I_H and fundamental I_1components, which are induced by nonlinear loads and will also be available further in the source current I_s. These components create disturbance, decrease efficiency, and stability within the power system. To mitigate this problem, the compensating current I_{inj} is injected into the power system affected by harmonics, according to the following relationship.

$$I_s = I_L - I_{inj} = (I_1 + I_H) - I_{inj} \tag{1}$$

According to the Eq. (1), the harmonic (I_H) and mitigation (I_{inj}) current will deduct each other and will remain the fundamental current

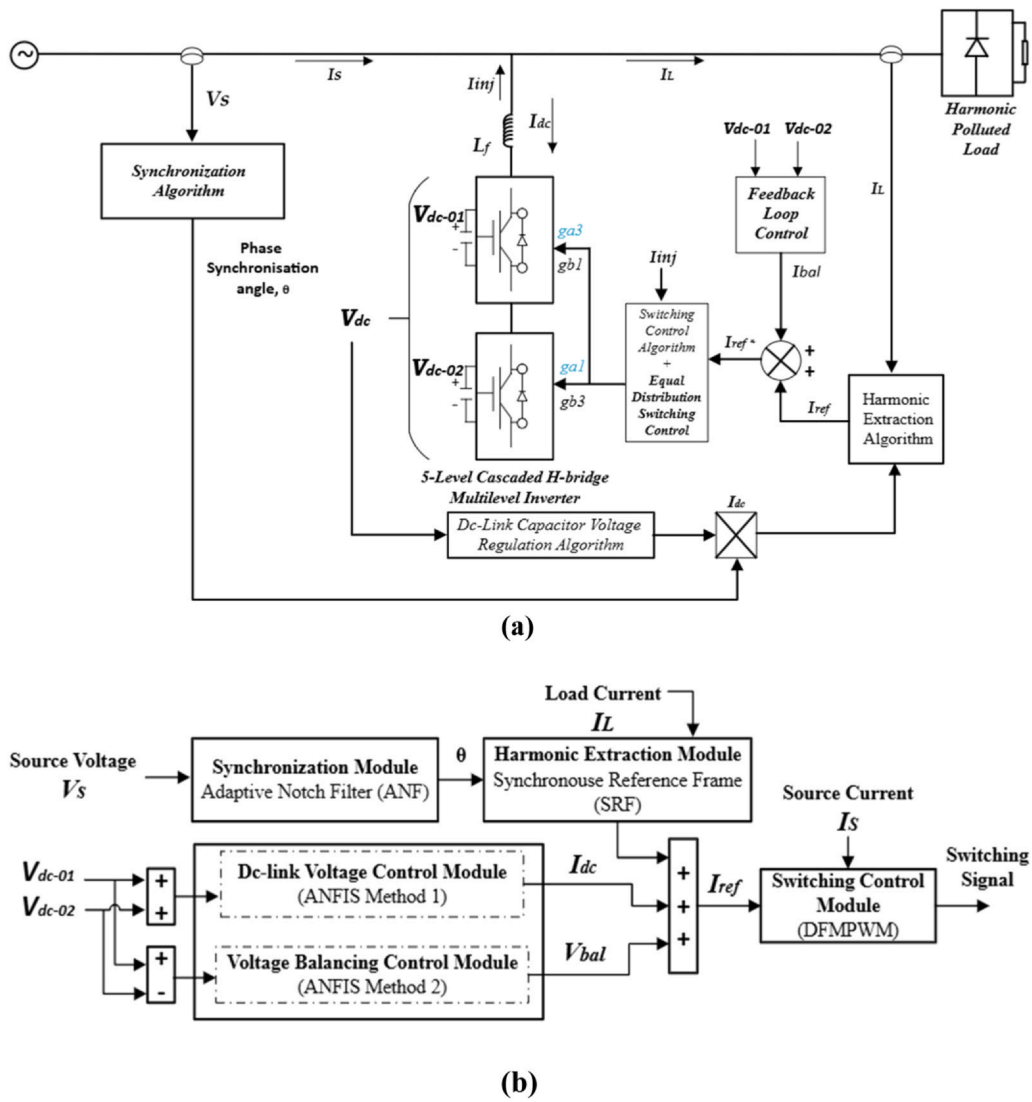

Fig. 2. SAPF based on 5-level CHB inverter: (a) Overview of control system (b) Algorithms applied for 5-level CHB inverter-based SAPF. ANFIS = adaptive neuro-fuzzy inference system; CHB = cascaded H-bridge; DFMPWM = dual-frequency multicarrier pulse width modulation; SAPF = shunt-active power filter.

I_1 within the source current I_s. In this manner, the system will be functioning in phase with the grid.

To control the operation of the SAPF inverter, 4 main techniques are employed: harmonic detection, Direct Current (DC) bus voltage regulation, capacitor voltage equalization, and gate pulse generation, as mentioned in Fig. 2(b). These methods are interconnected. In this study, the focus is on voltage balancing, which is elaborated in Section 3. The technique used to manage the generation of IGBT gate pulses is generally referred to as the switching or current control method [7]. Moreover, the Adaptive Neuro-Fuzzy Inference System (ANFIS) is utilized to control and stabilize the overall DC-link voltage. In Refs. [20–22], the efficacy of ANFIS is reported, particularly in achieving favorable outcomes in voltage regulation and balancing within MLIs. ANFIS is known for its ability to handle complex, dynamic systems and transient response, and demonstrates notable success in enhancing the precision and adaptability of control mechanisms. Its utilization in switching applications not only reflects its versatility but also underscores its potential to address challenges related to voltage control, making it a compelling choice for advancing control strategies in diverse contexts, including MLI systems.

In operation, the control strategy is carried out in several stages. Initially, the harmonic extraction technique is utilized to identify and isolate the harmonic content from the load current I_L. The harmonic current estimation is performed using the Synchronous Reference Frame (SRF) method. This method offers enhanced active and reactive power control under dynamic load conditions in the balanced systems [23]. The measured current I_L is first converted into a 2-axis $(\alpha - \beta)$ system using an orthogonal signal generation technique. The grid phase angle, obtained from a phase-locked loop (PLL), is then used to transform these currents into a rotating d-q reference frame through Park transformation. In this synchronous frame, the fundamental component of the load current is converted into a DC quantity, whereas the harmonic component appears as Alternating Current (AC) ripple components. By applying an allow pass filter to the D-axis current, the DC component corresponding to the fundamental active current is extracted. The harmonic currents are estimated by subtracting this fundamental component from the total current in the synchronous frame, thereby isolating the oscillatory harmonic component.

The reference compensating current is generated based on this extracted harmonic component. Additionally, the DC-link voltage controller processes the voltage error to produce an active current component required to maintain the DC-link voltage at its reference value. This component is combined with the extracted signals in the d-q frame to perform the final reference current (I_{ref}). The reference currents are then transformed back to the stationary frame using the inverse Park transformation, producing the reference compensating current that the

SAPF must inject. By forcing the inverter current to track this reference, the source current becomes sinusoidal, balanced, and free of harmonic distortion [4,31].

Simultaneously, a voltage handling unit in this module carries out grid synchronization by transforming the input voltage V_s into a unity sinusoidal waveform. Concurrently, V_{dc-01} and V_{dc-02} , which is voltage regulation across each H-bridge is designed by 2 ANFIS controllers to generate 2 currents I_{bal} and I_{dc}, required for voltage balancing and capacitor charging. For the reference current signal I_{ref}, it is derived by utilizing the extracted harmonic data, estimated current I_{bal} and I_{dc}, and the unity since function. For system stability, the reference current I_{ref} is then compared with the measured source current I_s , and finally, to minimize the error between I_{ref} and I_s, the switching control method will be applied to manage the operation of 5-level CHB inverter.

3. Methodology

The architecture of the suggested controller is detailed in Subsection 3.1, presented the problem scheme of the existing method. In Subsection 3.2, an overview of the generation of the gate pulses switching algorithm. In Subsection 3.3, discussed the structure and control scheme of proposed algorithm. In Subsection 3.4, discussed the configuration of the proposed algorithm. In Subsection 3.5, discusses the equation for the selection of parameters.

3.1. Conventional PI controller

To attain effective voltage balancing, the integration of a feedback control mechanism is necessary. This is because the equal distribution switching technique cannot provide identical output voltage steps for the lower and upper H-bridge cells, resulting in minor discrepancies. Hence, feedback control is utilized to minimize these deviations. To minimize these effects, it is crucial to develop a voltage balancing algorithm that is more efficient in both steady and transient responses in comparison to the PI controller. This algorithm usually applies because of a straightforward structure and is used to enhance the overall voltage stabilization across the capacitors represented as V_{dc-01} and V_{dc-02}, which is typically crucial in an ideal condition. These issues make the system unstable due to uneven switching stress on the capacitor, diminished inverter performance, and increased in harmonic distortion. Therefore, achieving and sustaining voltage balance is of paramount importance for the effective operation of a SAPF.

The structure shown in Fig. 3, consist straight forward techniques and has a fast response, but PI cannot handle when a nonlinear load occurs. To mitigate these challenges, this project introduces the implementation of an adaptive neural fuzzy interference system ANFIS, this algorithm has the capability to mitigate the nonlinear load condition and has fast dynamic and steady state response.

3.2. Overview of switching control algorithm

To address the voltage imbalance in each DC-link capacitor, identifying the root cause is essential. The main factor behind these imbalance problems is the control parameter of the signals that operate the IGBT's. An uneven distribution of switching sequences results in irregular charging and discharging of the inverter's DC-link capacitors,

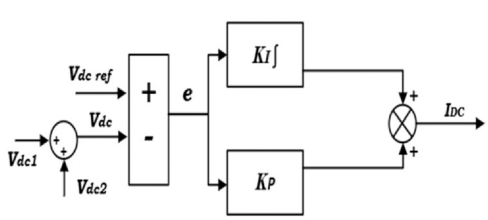

Fig. 3. Structure of PI controller. PI = proportional integral.

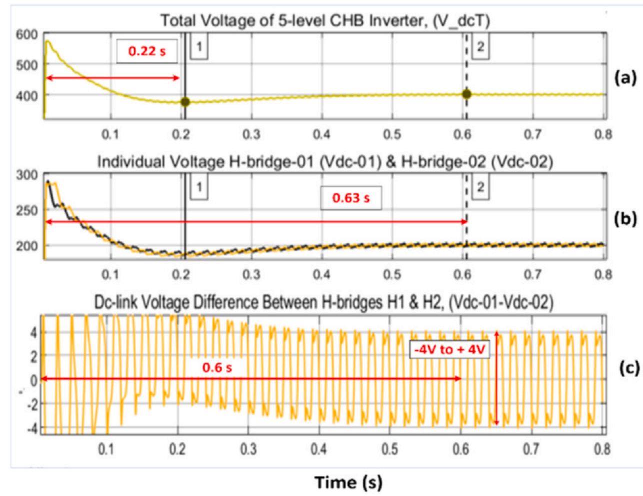

Fig. 4. Waveform overall Dc-link voltages: Total voltage of 5-level CHB inverter, V_{dcT} (b) Individual voltages V_{dc-01} & V_{dc-02} (c) Dc-link voltage difference ($V_{dc-01}-$ V_{dc-02}). CHB = cascaded H-bridge.

which in turn amplifies both transient and steady-state responses. In addition, both Dc-link capacitors experience voltage imbalance problems in the 5-level CHB inverter. Moreover, Fig. 4 demonstrates the overall voltage waveform of the existing PI controller method, along with the overall voltage of the 5-level CHB inverter, individual voltages V_{dc-01} and V_{dc-02} and variation between the voltages ($V_{dc-01}-V_{dc-02}$). It is clear from Fig. 4(a) that at 0.22 s, the total voltage V_{dcT} decreases to approximately 390 V of V_{dcT} and 180 V ($V_{dc-01}-V_{dc-02}$)and then settles down at 0.63 s as shown in Fig. 4(a) and Fig. 4(b). Meanwhile, the DC ripple is observed to oscillate between 4 V to -4V as shown in Fig. 4(c). This comparison shows that the PI controller is less efficient and still needs to enhance stability with fast dynamic and steady state response by configuring the control signal.

To mitigate the above challenges, as illustrated in Fig. 4, Fig. 1(b) shows a power control configuration for the 5-level CHB inverter SAPF application with a uniform switching pattern. This system consists of 2 H-bridge modules connected in series, each consisting of 4 switches and supported by Dc voltages with equal magnitude in symmetrical operation. The 3 voltage steps are generated by each H-bridge module that is ($+V_{dc}$, 0, -V_{dc}), and the final voltage steps should be ($+2V_{dc}$, 0, -$2V_{dc}$) with 5 voltage steps [1,24]. This uniform pattern enables the switches in each module to operate with appropriate on and off durations. However, when voltage steps are generated using the conventional method, the switching sequence becomes irregular, leading to imbalance issues within the power system of each H-bridge module. As illustrated in Fig. 1(a), the switching pattern is unevenly distributed, causing both H-bridge modules to conduct unequally [25]. The distribution of the even switching pattern is represented 'H' is input high and 'L' is low input, as shown in Table 1.

3.3. Working concept of ANFIS

In addition, ANFIS is used in some works showing its merits over other fuzzy-based algorithms. The study proves its robustness in Dc-link voltage regulation, adaptive learning capability that enables effective compensation of harmonic currents generated by nonlinear loads, resulting in a significant reduction of source current total harmonic distortion (THD). Furthermore, it highlights improved enhancement during load variation and output waveform quality [26–28]. controller enhances reactive power compensation and power factor correction while maintaining stable DC-link voltage under nonlinear load conditions, achieving a reduction in source current distortion and improved compensation dynamics during load variation [29]. This algorithm can model nonlinear relationships effectively with relatively small datasets,

Table 1
Switching pattern for 5-level cascaded H-bridge inverter

S_{23}				S_{11} Output (V) H_1	S_{13} Output (V) H_2	S_{21} Total (V), H_1 & H_2
H	L	H	L	$+V_{dc}$	$+V_{dc}$	$+2V_{dc}$
H	L	L	L	$+V_{dc}$	0	$+V_{dc}$
H	L	H	H	$+V_{dc}$	0	
L	L	H	L	0	$+V_{dc}$	
H	H	H	L	0	$+V_{dc}$	
L	L	L	L	0	0	0
L	L	H	H	0	0	
H	H	H	H	0	0	
H	H	L	L	0	0	
H	L	L	H	$+V_{dc}$	$-V_{dc}$	
L	H	H	L	$-V_{dc}$	$+V_{dc}$	
L	H	L	L	$-V_{dc}$	0	$-V_{dc}$
L	H	H	H	$-V_{dc}$	0	$-V_{dc}$
L	L	L	H	0	$-V_{dc}$	
H	H	L	H	0	$-V_{dc}$	
L	H	L	H	0	$-V_{dc}$	$-2V_{dc}$

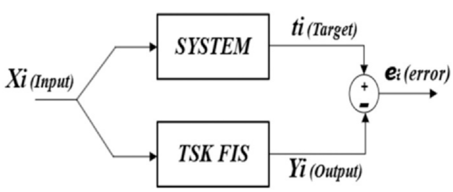

Fig. 5. Block diagram of ANFIS. ANFIS = adaptive neuro-fuzzy inference system.

incorporating human expertise through fuzzy rules and offering good generalization in uncertain environments [30]. The ANFIS is a flexible, learning-based network structured around the conventional fuzzy inference framework, and a comprehensive description can be found in [31]. It utilizes a first-order Takagi Sugeno Kang fuzzy model, which initially forms a basic fuzzy system and then employs learning algorithms to minimize the error to zero [32]. Fig. 5 presents the block diagram illustrating its ability to improve system stability while maintaining minimal error [33,34].

By adjusting the model parameters, its behavior can be matched to that of the real system. To achieve this, the mean square error (MSE) is employed as the cost function [35].

$$\mathrm{MSE} = \frac{1}{N} = \sum_{i=1}^{N} e_i^2 \tag{2}$$

Eq. (2) defines e as the error value, i as the index representing each sample, and N as the total number of data points. The model parameters are adjusted so that the cost function reaches its minimum value, a process known as training. The input-output relationship of the fuzzy model is represented in Eq. (3).

$$y_i = \frac{\sum_{l=1}^{m} y^{-l} \prod_{i=1}^{n} e^{-\left(\frac{x_i - m_i^l}{\sigma_i^l}\right)^2}}{\sum_{l=1}^{m} \prod_{i=1}^{n} e^{-\left(\frac{x_i - m_i^l}{\sigma_i^l}\right)^2}} \tag{3}$$

The Eq. (3), y_i represents the output, while x_i denotes the input of the controller. The parameters m_i^l and σ_i^l correspond to the Gaussian membership function parameters, commonly referred to as tuneable parameters, which are adjusted to minimize the cost function. Whereas, l indicates the quantity of fuzzy rules ranging from 1, ……, m, and n represents the total amount of data points ranging from 1, ……, i. Consider, if $w^l = \prod_{i=1}^{n} \exp\left(-\left(\frac{x_i - m_i^l}{\sigma_i^l}\right)^2\right)$ as an approximation in Eq. (3),

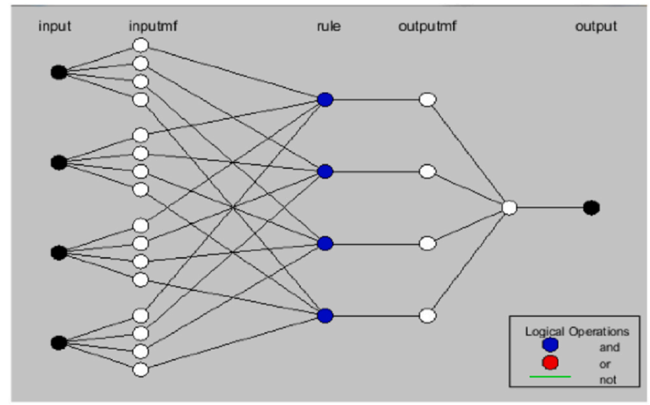

Fig. 6. Control structure of ANFIS. ANFIS = adaptive neuro-fuzzy inference system.

then the cost function will be written as below in Eq.(4).

$$y_i \frac{\sum_{l=1}^{m} y^{-l} w^l}{\sum_{l=1}^{m} y^{-l}} = \frac{a}{b} \tag{4}$$

$$\mathrm{E} = \frac{1}{N} \sum_{i=1}^{N} e_i^2 = \frac{1}{N}(t_i - \quad y_i)^2 \tag{5}$$

In Eq. (6), a and b are approximated by utilizing the descending gradient method, Eq. (5) also be drive by a differential equation. In Eq. (5), t_i and y_i represented as the desired value and the resulting output of the ANFIS controller as shown in Fig. 6, and the parameter m_i^l can be described as shown in Eq. (6) and Eq. (7).

$$\frac{\partial E}{\partial m_l^i} = \frac{\partial E}{\partial y_i}\left(\frac{\partial y_i}{\partial a} \times \frac{\partial a}{\partial w^l} \times \frac{\partial w^l}{\partial m_i^l} + \frac{\partial y_i}{\partial b} \times \frac{\partial b}{\partial w^l} \times \frac{\partial w^l}{\partial m_i^l}\right)$$

$$\frac{\partial E}{\partial m_l^i} = \frac{-2(t_i - y_i)}{N}\left(\frac{1}{b} \times y^{-l} \times 2\left(\frac{x_i - m_i^l}{(\sigma_i^l)^2}\right)w^l - \frac{a}{b^2} \times 1 \times 2\left(\frac{x_i - m_i^l}{(\sigma_i^l)^2}\right)w^l\right)$$

$$\frac{\partial E}{\partial m_l^i} = \frac{-4(t_i - \quad y_i)}{N}\left(\frac{x_i - m_i^l}{(\sigma_i^l)^2}\right)w^l(y^{-l} - y^i) \tag{6}$$

$$m_i^l(K+1) = m_i^l(k) - \alpha \frac{\partial E}{\partial m_i^l} \tag{7}$$

According to Eq. (7), α is the learning rate coefficient that adjusts according to the descending gradient method in ANFIS, aiming to optimize the controller parameters. For the parameter of σ_i^l, it can be represented as follows.

$$\frac{\partial E}{\partial \sigma_i^l} = \frac{\partial E}{\partial y_i}\left(\frac{\partial y_i}{\partial a} \times \frac{\partial a}{\partial w^l} \times \frac{\partial w^l}{\partial m_i^l} + \frac{\partial y_i}{\partial b} \times \frac{\partial b}{\partial w^l} \times \frac{\partial w^l}{\partial m_i^l}\right)$$

$$\frac{\partial E}{\partial \sigma_i^l} = \frac{-2(t_i - y_i)}{N}\left(\frac{1}{b} \times y^{-l} \times 2\left(\frac{(x_i - m_i^l)^2}{(\sigma_i^l)^3}\right)w^l - \frac{a}{b^2} \times 1 \times 2\left(\frac{(x_i - m_i^l)^2}{(\sigma_i^l)^3}\right)w^l\right)$$

$$\frac{\partial E}{\partial \sigma_i^l} = \frac{-4(t_i - y_i)}{Nb}\left(\frac{(x_i - m_i^l)^2}{(\sigma_i^l)^3}\right)w^l(y^{-l} - y^i) \tag{8}$$

$$\sigma_i^l(\mathrm{k}+1) = \sigma_i^l(k) - \alpha \frac{\partial E}{\partial \sigma_i^l} \tag{9}$$

The Fuzzy C-Means clustering technique is utilized for the initial fuzzy system. This approach enables each data point to be associated

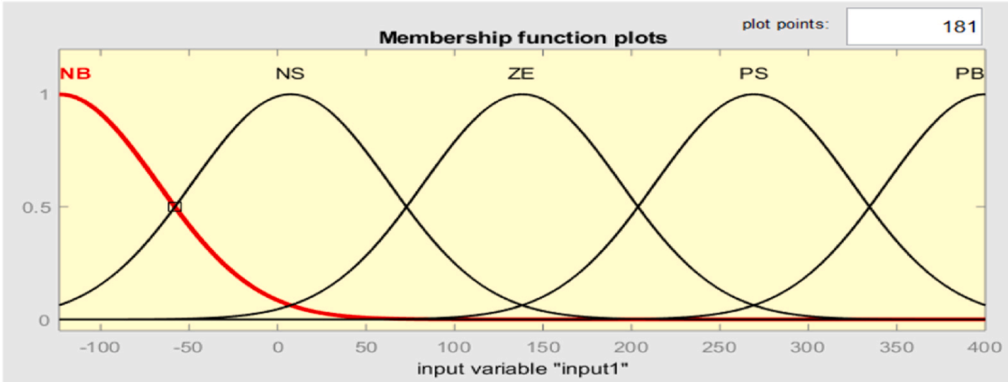

Fig. 7. Membership function of fuzzy.

with several clusters simultaneously, each with a different membership value. It is commonly applied to minimize the cost function.

$$J_m = \sum_{i=1}^{D} \sum_{j=1}^{N} \mu_{ij}^{m} \ \|x_i - c_j\|^2 \tag{10}$$

In Eq. (10), D represents the total number of data points, where N is the number of clusters, x_i is the i^{th} data point, C_j is the center of j^{th} cluster, and μ_{ij}^{m} indicates the membership degree of x_i in the j^{th} cluster. The cluster equation is written as follows.

$$c_j = \frac{\sum_{i=1}^{D} \mu_{ij}^{m} x_i}{\sum_{i=1}^{D} \mu_{ij}^{m}} \tag{11}$$

3.4. Configuration of proposed algorithm

Fig. 6 shows the internal structure of ANFIS, which contains 4 steps, in the first step required new data pairs, second step training of the data pair is required, third step is to decide the membership function and epochs and in last fourth step testing the train data. The more you apply membership function and epochs the system gets more efficient and more stable, but the processing and computational work would also be increased. The SAPF has effectively functioned with remarkable mitigation capabilities by adding benefits of ANFIS. However, there are only a few works focusing on the use of ANFIS in voltage balancing control that have been documented. This may be because integrating them is tough and complex, especially when it comes to ensuring compatibility between voltage balancing and the accompanying current control approaches. In addition, careful parameter adjustment is still necessary for ANFIS design, and the optimization process usually involves a difficult iterative process.

Furthermore, Fig. 7 illustrates the fuzzification process, where the input parameters are converted into their linguistic representations through corresponding fuzzy membership functions. The Gaussian membership function is used in this case. Based on the training data, fuzzy rules are formulated to describe the mapping between the input and output control actions, as illustrated in Fig. 8, followed by the defuzzification stage. After defuzzification, the fuzzy output is transformed into a numerical control signal. This procedure represents the ANFIS mechanism for regulating voltage deviations within the system. The internally structured rules are outlined as follows.

1. If the voltage difference $(V_{dc-01} - V_{dc-02})$ is NB, the output is NB, "negative big".
2. If the voltage difference $(V_{dc-01} - V_{dc-02})$ is NS, the output is NS, "negative small".
3. If the voltage difference $(V_{dc-01} - V_{dc-02})$ is ZE, the output is ZE, "zero".
4. If the voltage difference $(V_{dc-01} - V_{dc-02})$ is PS, the output is PS, "positive small".

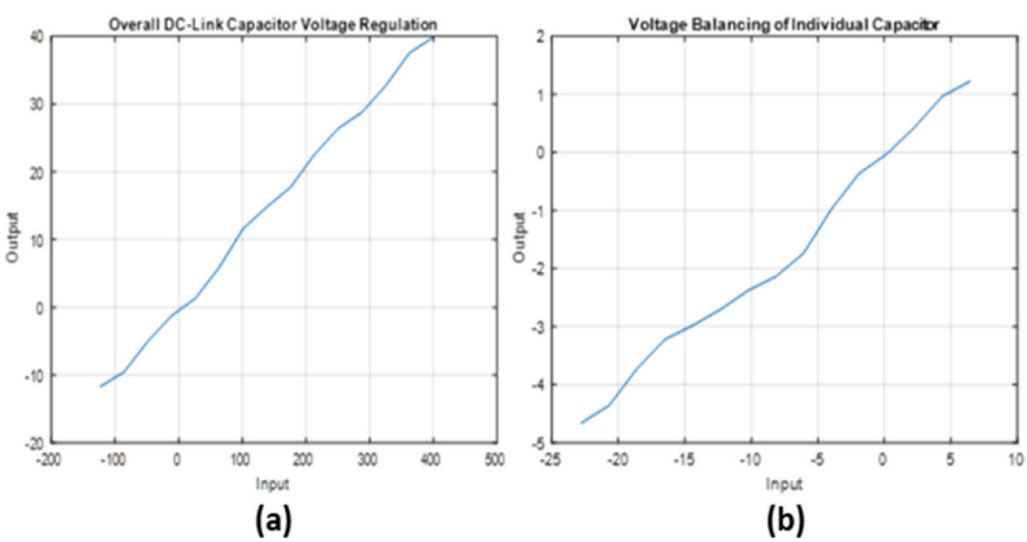

Fig. 8. Input and output relationship of the capacitor and voltage balancing: (a) Total DC-link capacitor voltage stabilization (b) Voltage stabilization of individual capacitors.

Table 2
Control parameter of power circuit

Parameters	Value
Ideal supply, V_s	230 V, 50 Hz
Distorted supply, V_s (THD =8.49%)	Fundamental component 230 V3rd Harmonic component 20 V5th Harmonic component10V7th Harmonic component 15 V9th Harmonic component 5 V
Dc link voltage, V_{dc}	400 V
Individual H-bridges (V_{dc-01} & V_{dc-02})voltage	200 V
Dc link capacitor, V_{dc} (C_1 and C_2)	4700 μF
Load resistor, R_L	25Ω
Load capacitor, C_L	1100μF
Load inductor, L_L Filter inductor	160 mH 3 mH
Choke inductor	1 mH
Switching frequency, f_s	5 kHz

5. If the voltage difference ($V_{dc-01} - V_{dc-02}$) is PB, the output is PB, “positive big”.

3.5. Design of power circuit parameters

3.5.1. Selection of DC-link voltage V_{dc} and filter inductor L_f

The function of the DC-link capacitor is to serve as an energy storage element that maintains a DC voltage for the inverter, enabling it to generate the required I_{inj} current to the I_s current. In conventional systems, a PI controller regulates the DC-link voltage by comparing the instantaneous voltage with its reference value. However, this approach may not ensure precise voltage regulation, leading to fluctuations in the DC-link voltage and consequently affecting the quality of the output voltage. To ensure adequate Dc-link voltage for effective compensation, the following condition must be satisfied:

$$V_{c,\max} = \frac{m}{2} V_{dc} \tag{12}$$

$V_{c,\max}$ represents the peak value of the system output voltage, V_{dc} represent Dc-link voltage, and m is the modulation index, which will be $0<m \leq 1$. The selection of the modulation index is very important because if the DC-link voltage is high, the inverter can only generate the limited AC voltage depending on the modulation index.

For stable operation, the DC-link capacitor voltage should be maintained at a level exceeding two-thirds of the grid voltage to ensure proper generation of the compensating current. The minimum required capacitance value can be calculated as follows:

$$\mathrm{C} \geq \frac{\max \left| \int_0^t I_{inj}(t) \right|}{\Delta V_{C\max}} \tag{13}$$

Where the above equation represented as,

I_{inj} is the injection current, and $\Delta V_{C\max}$ is the maximum ripple voltage of the DC-link capacitor. Furthermore, during the charging process, as discussed in the introduction, the voltage of the DC-link capacitor always changes from the desired voltages, which contributes to the difference in energy storage ΔE in the DC-link capacitor is represented as below.

$$\Delta E = \frac{C}{2}\left[(V_{dc-02})^2 - (V_{dc-01})^2\right] \tag{14}$$

In Eq. (13), C represents the capacitance value, V_{dc-01} corresponds to the reference Dc-link voltage, V_{dc-02} represents the instantaneous Dc-link voltage. The energy supplied by the single-phase AC system to charge the capacitor, E_{ac} can be expressed as follows,

$$E_{ac} = Pt_c$$

$$E_{ac} = V_{rms} I_{dc} \cos\theta t_c \tag{15}$$

Where P is the real power, t_c is the capacitor charging time, V_{rms} is the value of supply voltage, I_{dc} is the charging capacitor current, θ is the difference of phase angle within the supply voltage and charging capacitor current and t_c can be represent as $\frac{T}{2}$, where T is the time period of the supply frequency which is 5 kHz. If we neglect the switching losses according to the law of energy conservation, the equation yields [36,37]:

$$\Delta E = E_{ac}$$

$$\frac{C}{2}\left[(V_{dc-02})^2 - (V_{dc-01})^2\right] = \frac{VI_{dc}T}{4}$$

$$\therefore I_{dc} = \frac{2C\left[(V_{dc-02})^2 - (V_{dc-01})^2\right]}{VT} \tag{16}$$

The filtering inductor (L_f) is used to attenuate the ripples of the filter current due to the switching of the converter. This inductor limits the compensating current ripple, ensures stable current control, and decouples the inverter switching harmonics from the grid. Hence, the design of L_f is based on the principle of harmonic current reduction, and the equation for SAPF is defined as:

$$L_f = \frac{V_{dc}}{2f_s \Delta i_c} \tag{17}$$

4. Comparative analysis of the proposed algorithm

Additionally, to assess the performance analyses of the MI-APF, a detailed evaluation of its steady-state conditions for both Resistor Capacitor (RC) and Resistor Inductor (RL) loads under ideal and distorted supply conditions is presented. Table 2 outlines the simulation parameters employed in MATLAB Simulink.

4.1. Steady- state analysis

The analysis compares the analysis of the existing control method with the proposed approach, highlighting improvements in the form of (V_{pp}) peak-peak voltage swing (voltage ripples), ($V_{\max}$) maximum overshoot, as can be observed from Figs. 9–12, the reduction of V_{pp} as also shown in Table 3.

Figs. 9 and 10 shows the total voltage of 5-level CHB inverter V_{dcT}, individual H-bridge voltage V_{dc-01} and V_{dc-02} and the voltage deviation (ΔV) within the Dc-link voltage ($V_{dc-01} - V_{dc-02}$) considering ideal and distorted supply under RC load, while Fig. 11 and Fig. 12 shows the total voltage of 5-level CHB inverter V_{dcT}, individual H-bridge voltage V_{dc-01} and V_{dc-02} and the voltage deviation (ΔV) within the Dc-link voltage ($V_{dc-01} - V_{dc-02}$) considering ideal and distorted supply under RL load. Furthermore, it is demonstrated that, the proposed method presented lesser V_{pp} of −5 V to +5.1 V and −4.1 V to +4.2 V for RC load and −2.1 V to +2.2 V is achieved from RL load under ideal and distorted supply. Meanwhile, the existing method presented a higher V_{pp} of −5.6 V to +5.5 V and −5.3 V to +5.3 V for RC load, while −4 V to +4 V and −3.8 V to +3.8 V for RL load under ideal and distorted supply as summarized in Table 3.

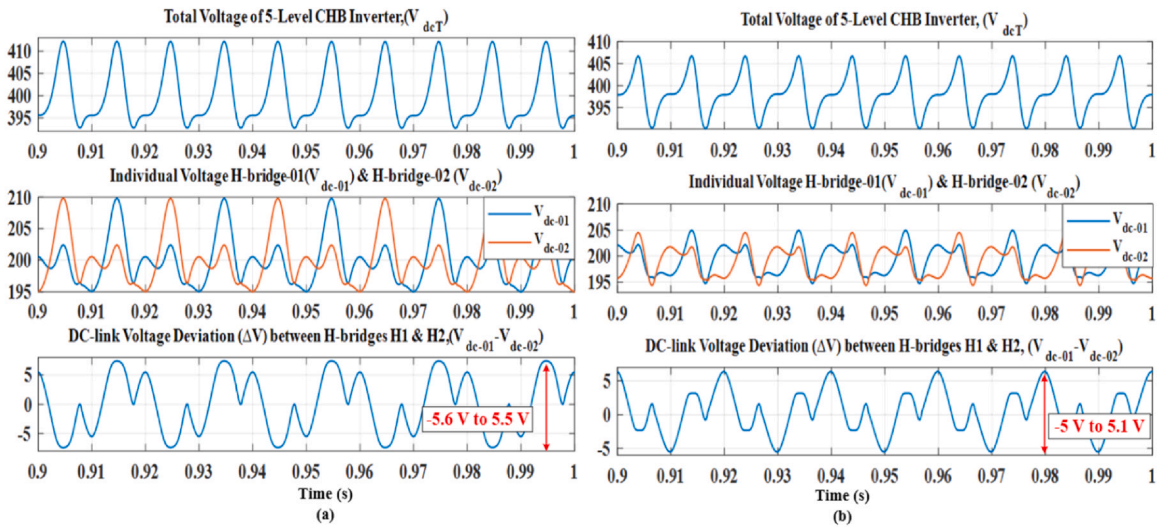

Fig. 9. Steady-state dc voltages waveforms obtained considering ideal supply and RC load, which include total Dc-link voltage V_{dc}, individual H-bridge voltage V_{dc-01} and V_{dc-02}, voltage difference ($V_{dc-01} - V_{dc-02}$)for: PI controller and (b) Proposed ANFIS method. ANFIS = adaptive neuro-fuzzy inference system; CHB = cascaded H-bridge; PI = proportional integral; RC = resistor capacitor.

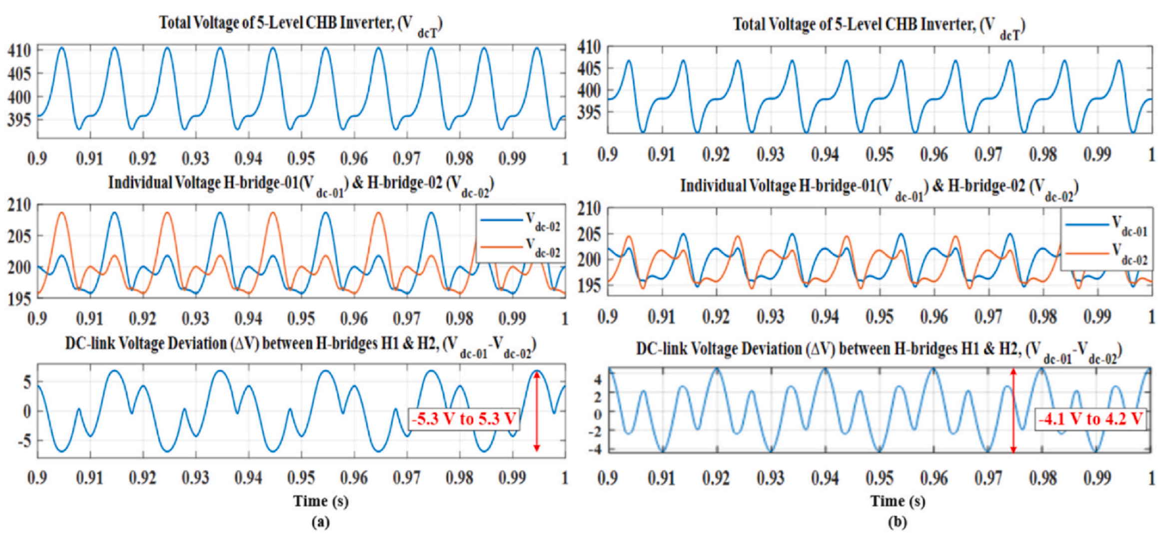

Fig. 10. Steady-state dc voltages waveforms obtained considering distorted supply and RC load, which include total Dc-link voltage V_{dc}, individual H-bridge voltage V_{dc-01} and V_{dc-02}, voltage difference ($V_{dc-01} - V_{dc-02}$)for: PI controller and (b) Proposed ANFIS method. ANFIS = adaptive neuro-fuzzy inference system; CHB = cascaded H-bridge; PI = proportional integral; RC = resistor capacitor.

4.2. Transient state analysis

Furthermore, it is depicted from Figs. 13–16, the PI controller regulates the Dc-link voltage up to the desired level, (t_s) response time at approximately 0.63 s with the maximum overshoot ($V_{\max}$) of V_{dcT} (620 V to 630 V), V_{dc-01}, V_{dc-02} (330 V to 340 V) and ΔV (50 V) with t_s (0.6 s) under RC load, while V_{dcT} (555 V to 580 V), V_{dc-01}, V_{dc-02} (280 V) and ΔV undershoot of (-31V to -33V) with t_s (0.41 s and 0.6 s), is observed under RL load condition. It is also analyze that after $V_{\max}$, DC-link voltages V_{dcT} and V_{dc-01}, V_{dc-02} decreases to 180 V approximately at t_s (0.1 s to 0.4 s) and starts to settled down after 0.5 s under both loads and supplies, whereas the ANFIS controller achieves the same target around 0.35 s with the $V_{\max}$ of V_{dcT} (530 V), V_{dc-01}, V_{dc-02} (255 V to 260 V) and ΔV (10 V to 11 V) with t_s (0.21 s) under RC load, while V_{dcT} (510 V to 530 V), V_{dc-01}, V_{dc-02} (255 V to 260 V) and ΔV undershoot of (-20V to -21V) with t_s (0.15 s and 0.21 s) is observed under RL load condition without any voltage variation within the Dc-link voltages, as shown in the highlighted results from Figs. 13–16 and summarized in Table 4, achieved under an ideal and distorted supply environment.

This analysis indicates that the proposed ANFIS approach responds nearly twice as fast as the conventional PI controller. In addition, ANFIS significantly reduces voltage ripples by 9.0% for the RC load and 46.26% for the RL load under ideal supply condition, ripple reduction further improves in both ideal and distorted supply environments, achieving 21.69% for the RC load and 42.10% for the RL load, as summarized in Table 3. These results demonstrate that the proposed control strategy delivers superior dynamic performance and enhanced ripple mitigation compared to the existing method, confirming its overall effectiveness and efficiency.

Next, Figs. 17 and 18 present the voltage and current waveforms, including (V_s) source voltage, (I_L) load current, (I_{inj}) injection current, and (I_s) source current is shown for both RC and RL loads under ideal and distorted supply conditions. The findings indicate that the applied compensating current effectively reduces the harmonic content in the load current. Meanwhile, the results in Table 5, supported by Figs. 17 and 18, comparatively illustrate the mitigation performance of the SAPF. The waveforms show that all source currents maintain a sinusoidal shape and remain in-phase with the source voltage (V_s) under both ideal and distorted supply conditions. The findings clearly proved that the existing and the proposed method have effectively mitigated

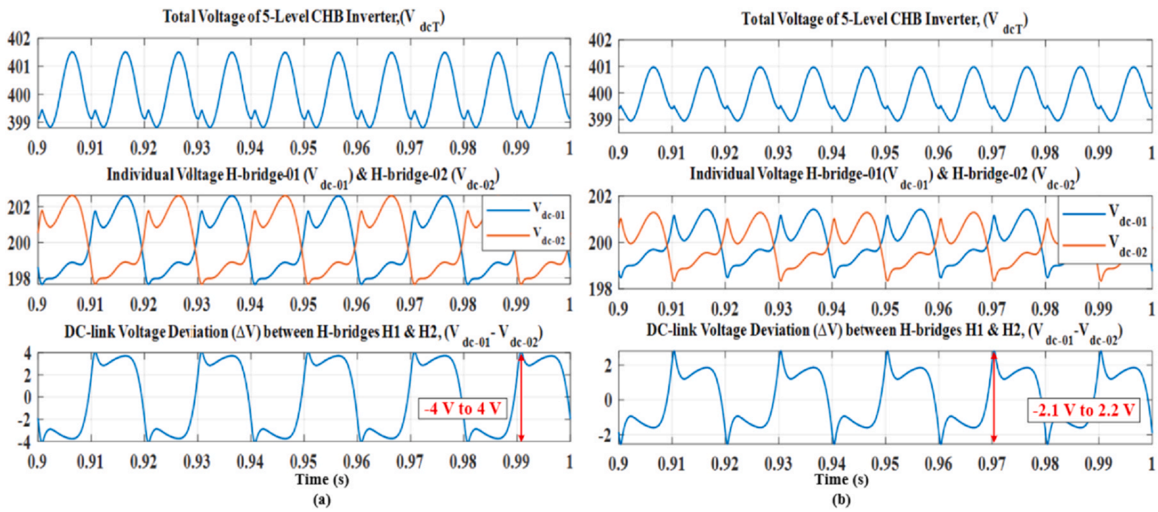

Fig. 11. Steady-state dc voltages waveforms obtained considering ideal supply and RL load, which include total Dc-link voltage's V_{dc}, individual H-bridge voltage V_{dc-01} and V_{dc-02}, voltage difference ($V_{dc-01} - V_{dc-02}$) for: (a) PI controller and (b) proposed ANFIS method. ANFIS = adaptive neuro-fuzzy inference system; CHB = cascaded H-bridge; PI = proportional integral; RL = resistor inductor.

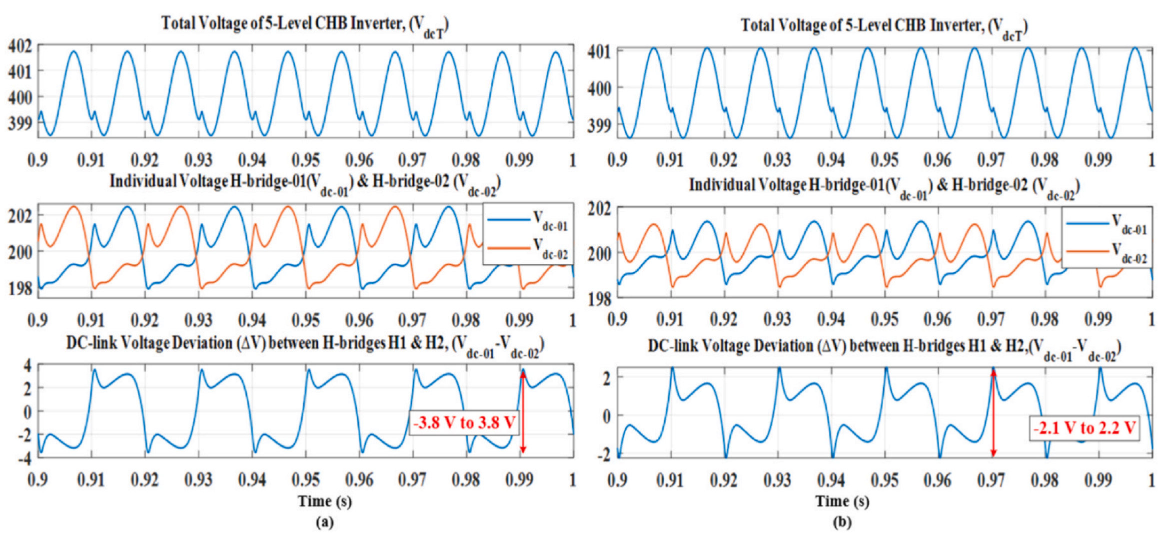

Fig. 12. Steady-state dc voltages waveforms obtained considering distorted supply and RL load, which include total Dc-link voltage's V_{dc}, individual H-bridge voltage V_{dc-01} and V_{dc-02}, voltage difference ($V_{dc-01} - V_{dc-02}$) for: PI controller and (b) proposed ANFIS method. ANFIS = adaptive neuro-fuzzy inference system; CHB = cascaded H-bridge; PI = proportional integral; RL = resistor inductor.

Table 3
Comparison of DC-link voltage (V) differences (V_{dc-01},V_{dc-02}) between PI and ANFIS

Condition	PI controller	ANFIS	% Reduction
Ideal supply, (V_{pp})			
▪ RC load	-5.6 V to +5.5 V(Total = 11.1 V)	-5 V to 5.1 V(Total = 10.1 V)	9.0%
▪ RL load	-4 V to 4 V(Total = 8.0 V)	-2.1 V to 2.2 V(Total = 4.3 V)	46.25%
Distorted supply, (V_{pp})			
▪ RC load	-5.3 V to 5.3 V(Total = 10.6 V)	-4.1 V to +4.2 V(Total = 8.3 V)	21.69%
▪ RL load	-3.8 V to +3.8 V(Total = 7.6 V)	-2.1 V to 2.2 V(Total = 4.4 V)	42.10%

ANFIS = adaptive neuro-fuzzy inference system; PI = proportional integral; RC = resistor capacitor; RL = resistor inductor.

current harmonics from both resistive and inductive loads, as summarized in Table 5.

4.3. Dynamic state analysis under 20% load reduction

This section discusses the performance of MI-APF under dynamic conditions. Figs. 19–21, illustrate the effectiveness of the proposed ANFIS controller when the load is decreased by 20% from the nominal value to 20Ω. Fig. 19 shows that the existing PI controller exhibits a higher Dc-link voltage ripple V_{pp}, ranging from −5 V to +5.1 V. In contrast, the proposed ANFIS controller achieves a significantly lower V_{pp} −2.8 V to +2.8 V, indicating improved ripple mitigation and enhanced voltage stability within the Dc-link.

Further analysis from Fig. 20 shows that the response time of the Dc-link i.e.V_{dcT} and V_{dc-01}, V_{dc-02} is 0.51 s using PI controller, with the voltage difference ΔV settling at approximately 0.5 s. Meanwhile, the

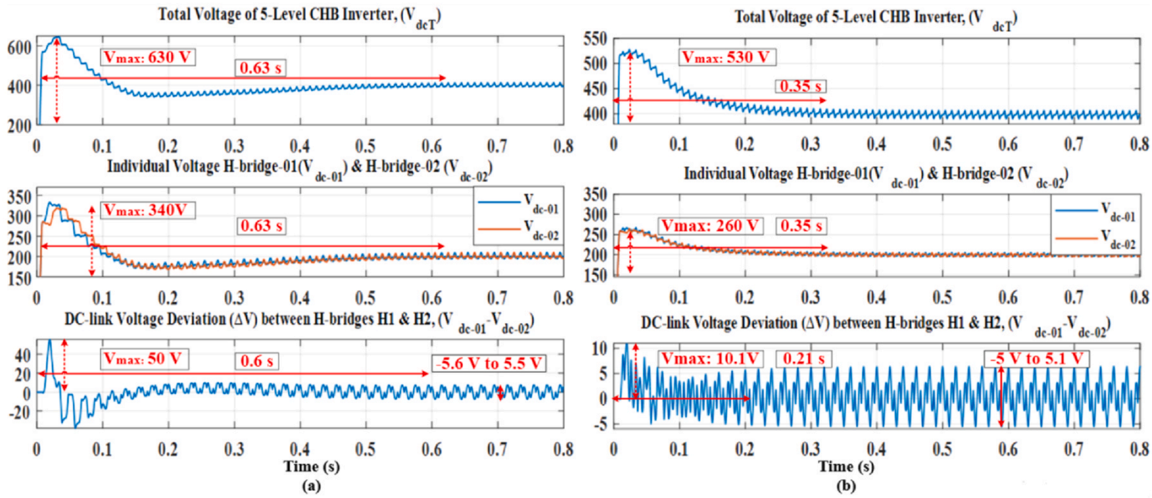

Fig. 13. Transient state comparison of Dc-link voltages, RC load under ideal supply: PI controller (b) ANFIS controller. ANFIS = adaptive neuro-fuzzy inference system; CHB = cascaded H-bridge; PI = proportional integral; RC = resistor capacitor.

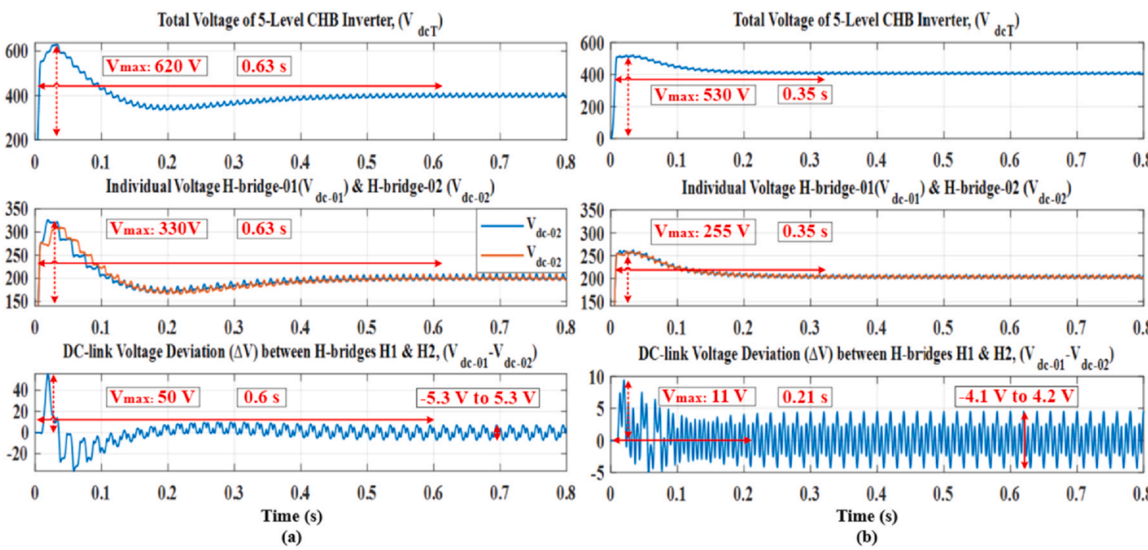

Fig. 14. Transient state comparison of Dc-link voltages, RC load under distorted supply: PI controller (b) ANFIS controller. ANFIS = adaptive neuro-fuzzy inference system; CHB = cascaded H-bridge; PI = proportional integral; RC = resistor capacitor.

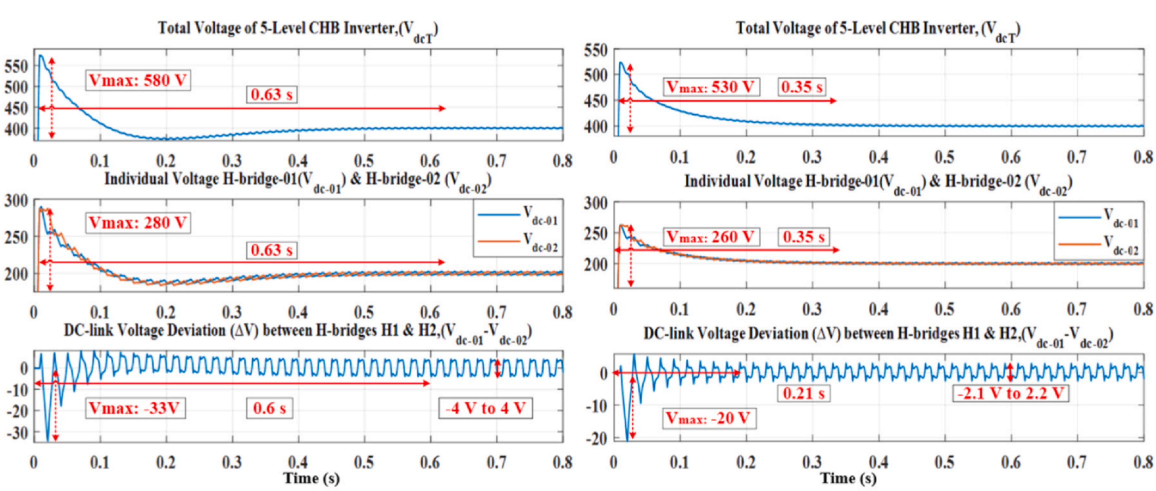

Fig. 15. Transient state comparison of Dc-link voltages, RL load under ideal supply: PI controller (b) ANFIS controller. ANFIS = adaptive neuro-fuzzy inference system; CHB = cascaded H-bridge; PI = proportional integral; RL = resistor inductor.

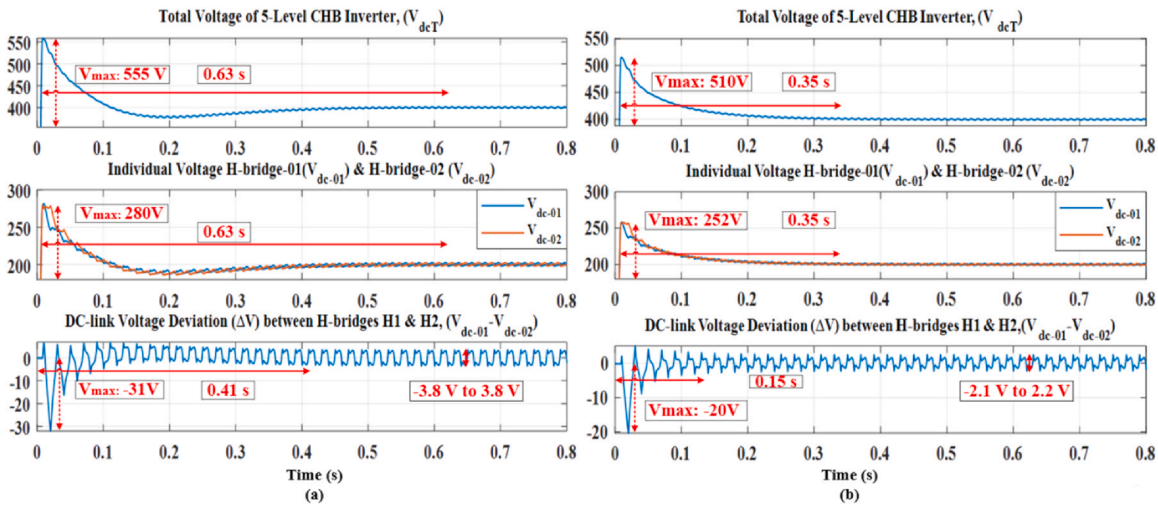

Fig. 16. Transient state comparison of Dc-link voltages, RL load under distorted supply: PI controller (b) ANFIS controller. ANFIS = adaptive neuro-fuzzy inference system; CHB = cascaded H-bridge; PI = proportional integral; RL = resistor inductor.

Table 4
Comparison of Dc-link response time (t_s), voltage overshoot (V_{max}) and % reduction

Condition			Ideal supply			Distorted supply		
			V_{dcT}	V_{dc-01},V_{dc-02}	V	V_{dcT}	V_{dc-01},V_{dc-02}	V
PI controller	t_s	RC	0.63 s	0.63 s	0.6 s	0.63 s	0.63 s	0.6 s
		RL	0.63 s	0.63 s	0.6 s	0.63 s	0.63 s	0.41 s
	V_{max}	RC	630 V	340 V	50 V	620 V	330 V	50 V
		RL	580 V	280 V	-33V	555 V	280 V	-31V
ANFIS	t_s	RC	0.35 s	0.35 s	0.21 s	0.35 s	0.35 s	0.21 s
		RL	0.35 s	0.35 s	0.21 s	0.35 s	0.35 s	0.15 s
	V_{max}	RC	530 V	260 V	10.1 V	530 V	255 V	11 V
		RL	530 V	260 V	-20V	510 V	252 V	-20V
% Reduction	t_s	RC	44.4%	44.4%	65.0%	44.4%	44.4%	65.0%
		RL	44.4%	44.4%	65.0%	44.4%	44.4%	63.4%
	V_{max}	RC	15.8%	23.5%	79.8%	14.5%	22.7%	78.0%
		RL	8.62%	7.14%	39.3%	8.10%	10.0%	35.4%

ANFIS = adaptive neuro-fuzzy inference system; PI = proportional integral; RC = resistor capacitor; RL = resistor inductor.

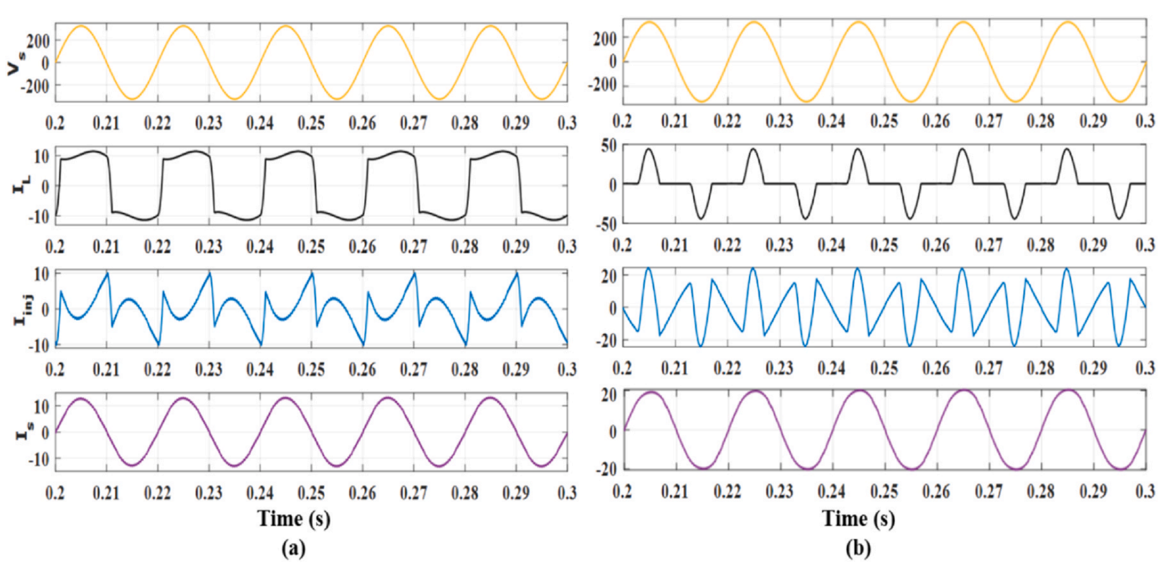

Fig. 17. Overall waveform of V_s, I_L, I_{inj}, I_s: RL load with ideal supply (b) RC load with ideal supply. RC = resistor capacitor; RL = resistor inductor.

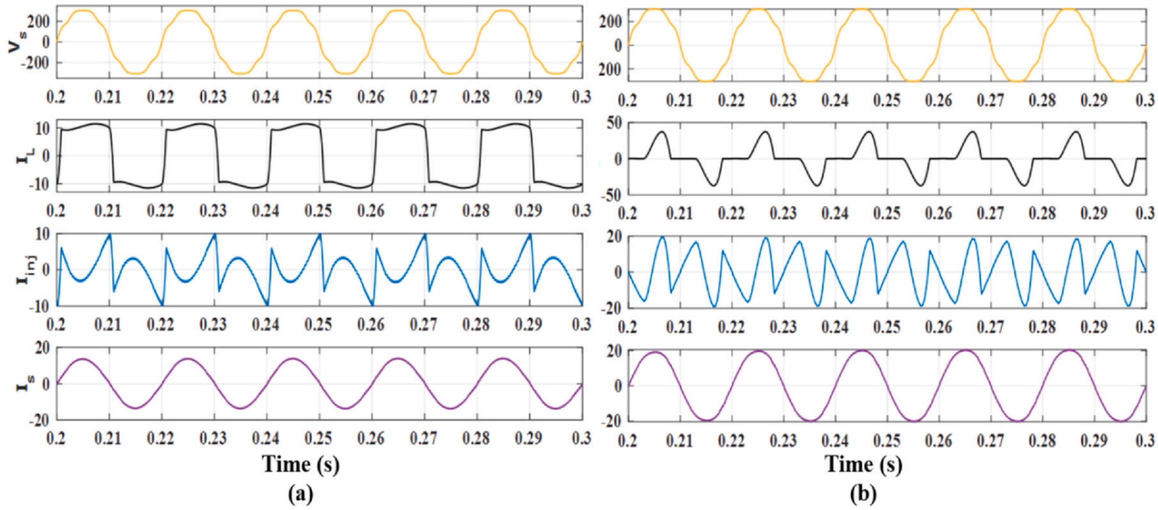

Fig. 18. Overall waveform of V_s, I_L, I_{inj}, I_s: RL load with distorted supply (b) RC load with distorted supply. RC = resistor capacitor; RL = resistor inductor.

Table 5
Total harmonic distortion (THD %) and phase difference (∅) between the load current (I_L) and source current (I_S) under different conditions

Current	Ideal supply			Distorted supply		
	PIcontroller	ANFIS	%Improvement	PIcontroller	ANFIS	%Improvement
RC load condition						
Load current, I_L	63.23	63.23	-	61.2	61.2	-
Source current, I_s	3.29	2.97	9.72%	3.50	3.27	6.57%
Power factor, P_f	0.999	0.999	-	0.999	0.999	-
Phase difference, P_d	0.4°	0.1°	75.0%	0.5°	0.2°	60.0%
RL load condition						
Load current, I_L	35.42	35.42	-	38.25	38.25	-
Source current, I_s	2.67	2.41	9.73%	3.31	3.03	8.45%
Power factor, P_f	0.999	0.999	-	0.999	0.999	-
Phase difference, P_d	0.4°	-0.1°	75.0%	0.5°	0.1°	80.0%

ANFIS = adaptive neuro-fuzzy inference system; PI = proportional integral; RC = resistor capacitor; RL = resistor inductor.

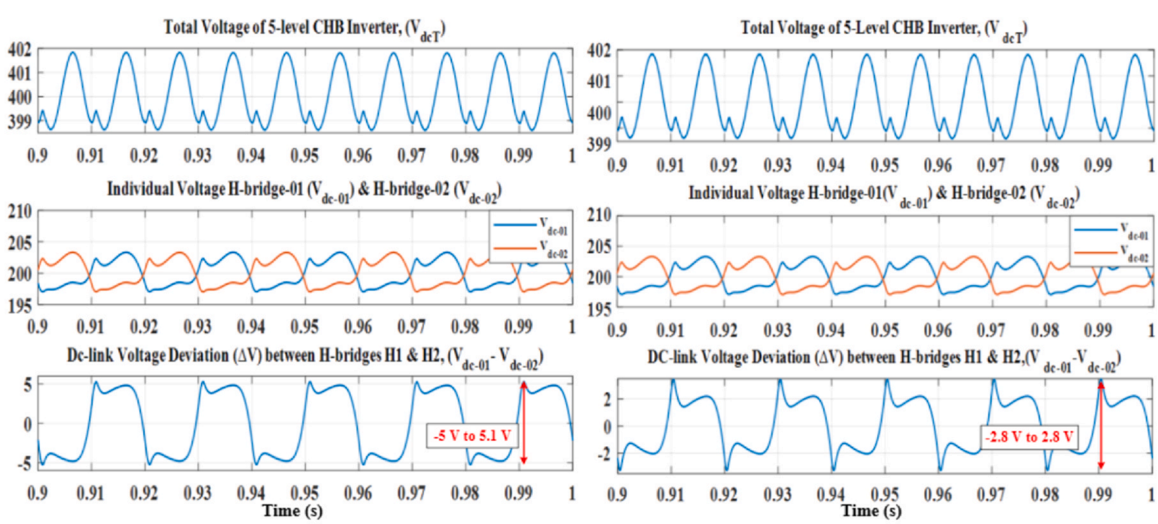

Fig. 19. Dc-link voltage performance after 20% load reduction: (a) PI controller and (b) proposed ANFIS method. ANFIS = adaptive neuro-fuzzy inference system; CHB = cascaded H-bridge; PI = proportional integral.

ANFIS controller achieves the same target in 0.32 s for V_{dcT} and V_{dc-01}, V_{dc-02}, while ΔV much faster at 0.1 s.

Overall, the proposed ANFIS controller reduces the response time of V_{dcT} and V_{dc-01}, V_{dc-02} by 37.25% and decreases the response time of ΔV by 80%, while maintaining stable Dc-link performance under RL load condition. These results demonstrate that the proposed control strategy provides superior dynamic performance and enhanced ripple mitigation compared to the conventional controller, confirming its robustness and overall effectiveness under load variation.

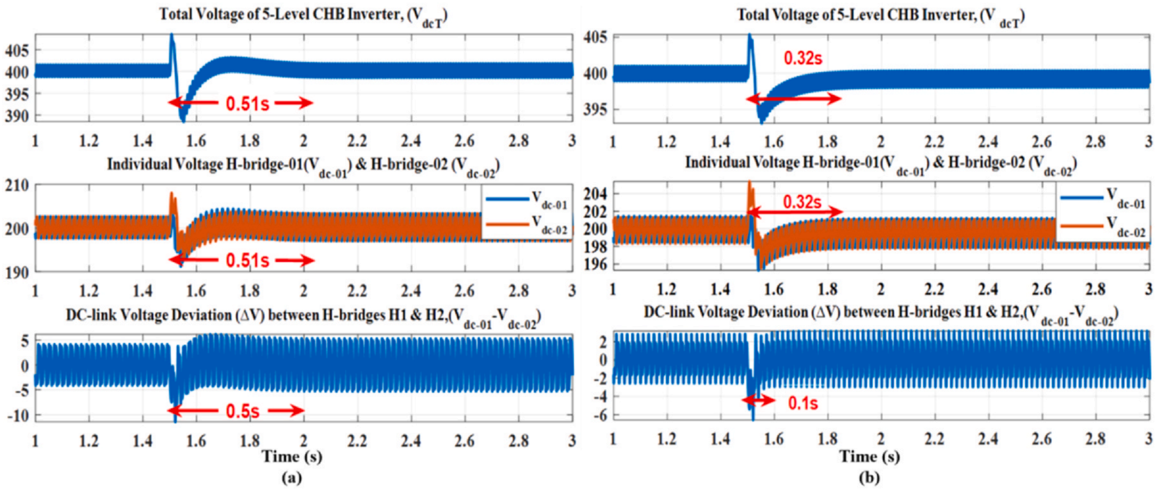

Fig. 20. Dynamic state comparison of Dc-link voltages under 20% load reduction: PI controller (b) ANFIS controller. ANFIS = adaptive neuro-fuzzy inference system; CHB = cascaded H-bridge; PI = proportional integral.

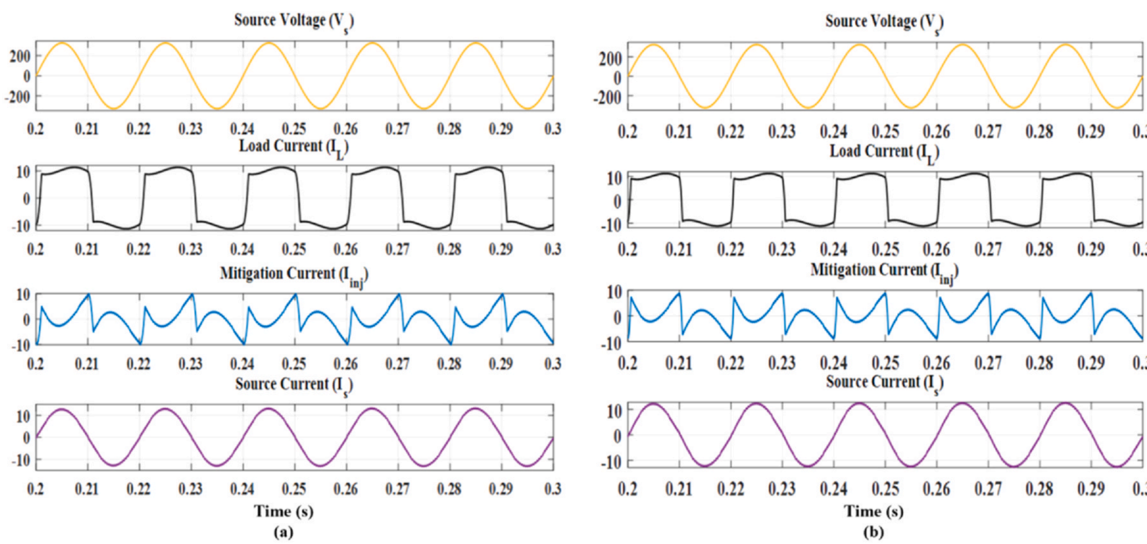

Fig. 21. Overall waveform of V_s, I_L, I_{inj}, I_s after 20% load reduction: PI controller (b) ANFIS controller. ANFIS = adaptive neuro-fuzzy inference system; PI = proportional integral.

4.4. Main achievement of the proposed ANFIS controller

Notably, the effectiveness of the proposed ANFIS controller is further validated through the reduction achieved in key performance parameters across various load and supply conditions. For the RC load under ideal supply, the ANFIS controller yields an improvement of 9.72% in source current (I_s), and 75.0% improvement in phase difference (P_d). Similarly, for the RL load under ideal supply, improvements of 9.73% in source current (I_s) and 75.0% in phase difference (P_d) are observed.

Specifically, under distorted supply conditions, the controller maintains its effectiveness. For the RC load, the optimization recorded are 6.57% in source current (I_s) and 60.0% in phase difference (P_d). In the case of the RL load, optimization of 8.45% in source current (I_s) and 80.0% in phase difference (P_d) are achieved. It is further tested after the load variation decreases 20%, that the system behaves with superior performance. The findings demonstrated that the proposed method ANFIS method exhibits superior performance compared to PI controller, achieving lower THD, minimal phase difference, no overshoot with fast response. These results collectively confirm that the ANFIS controller provides consistent and significant performance enhancement in terms of current quality, power factor correction, and phase alignment across different operating conditions.

5. Conclusions

In this work, the first improvement is to enhance the voltage balancing with minimal overshoot and response time by using ANFIS controller designed for a single-phase SAPF. It clearly shows from the above Table 3 and Table 4, the proposed adaptive neural fuzzy interference system (ANFIS) algorithm achieved a response time of 2 times faster compared to PI.

The proposed algorithm has demonstrated strong robustness in responding to sudden variations in load conditions, i.e., by achieving a response of 0.35 s with no overshoot and faster response time while maintaining an effective reduction of V_{pp} 9.0% and 21.69% under RC load, 46.25% and 42.10% under RL load, highlighting the effectiveness in both ideal and distorted supply conditions. Meanwhile, Table 5 demonstrated the mitigation performance of the currents and improvements of Source current (I_s), Phase difference (P_d). The proposed method is mainly designed to maintain the effectiveness when nonlinear load applied, i.e., optimization recorded are 6.57% in source current (I_s) and 60.0% in phase difference (P_d), while successfully maintaining the power factor. The results confirm the improved stability and performance achieved using the ANFIS algorithm in MLI systems. They highlight the effectiveness of ANFIS in practical applications, underlining its significant contribution to enhancing power performance and strengthening the dependability of contemporary power systems.

CRediT authorship contribution statement

Yap Hoon: Conceptualization, Data curation, Funding acquisition, Investigation, Methodology, Project administration, Resources, Software, Supervision, Validation, Visualization, Writing – review & editing. **Syed Zaki ul Hasan Naqvi:** Conceptualization, Data curation, Formal analysis, Investigation, Methodology, Validation, Visualization, Writing – original draft, Writing – review & editing, Software. **Mohd Amran Mohd Radzi:** Funding acquisition, Project administration, Resources, Supervision, Validation, Writing – review & editing. **KuewWai Chew:** Funding acquisition, Project administration, Resources, Supervision, Validation, Writing – review & editing.

Declaration of Competing Interest

The authors declare that they have no known competing financial interests or personal relationships that could have appeared to influence the work reported in this paper.

Acknowledgments

This research was supported by Ministry of Higher Education, Malaysia (MoHE), through Fundamental Research Grant Scheme (FRGS/1/2024/TK08/UTAR/02/4).

References

[1] J. Rodríguez, J.S. Lai, F.Z. Peng, Multilevel inverters: a survey of topologies, controls, and applications, IEEE Trans. Ind. Electron 49 (4) (2002) 724–738, https://doi.org/10.1109/TIE.2002.801052.

[2] H. Akagi, Active harmonic filters, Proc. IEEE 93 (12) (2005) 2128–2141, https://doi.org/10.1109/JPROC.2005.859603.

[3] Y. Ko, A. Tcai, M. Liserre, DC-link voltage balancing modulation for cascaded H-bridge converters, IEEE Access 9 (2021) 103524–103532, https://doi.org/10.1109/ACCESS.2021.3098896.

[4] Y. Hoon, M.A.M. Radzi, M.K. Hassan, N.F. Mailah, Three-phase three-level shunt active power filter with simplified synchronous reference frame. In: Proceedings of the 2016 IEEE Industrial Electronics and Applications Conference (IEACon), 2016. pp. 1-6. doi: 10.1109/IEACON.2016.8067346.

[5] L. Manai, D. Hakiri, M. Besbes, Backstepping control of flying capacitor multilevel inverter-based active power filter, IET Power Electron 13 (19) (2020) 4610–4624, https://doi.org/10.1049/iet-pel.2020.0734.

[6] O. Sánchez Vargas, L.G. Vela Valdés, M. Borunda, R.E. Lozoya-Ponce, J. Aguayo Alquicira, S.E. De León Aldaco, ANFIS-PSO-based optimization for THD reduction in cascaded multilevel inverter UPS systems, Electronics 13 (22) (2024) 4456, https://doi.org/10.3390/electronics13224456.

[7] Y. Hoon, M.A.M. Radzi, M.K. Hassan, N.F. Mailah, Control algorithms of shunt active power filter for harmonics mitigation: a review, Energies 10 (12) (2017) 2038, https://doi.org/10.3390/en10122038.

[8] K.T. Maheswari, R. Bharanikumar, V. Arjun, R. Amrish, M. Bhuvanesh, A comprehensive review on cascaded H-bridge multilevel inverter for medium voltage high power applications, Mater. Today Proc. 46 (2021) 2666–2670, https://doi.org/10.1016/j.matpr.2020.11.519.

[9] M. Malinowski, K. Gopakumar, J. Rodríguez, M.A. Pérez, A survey on cascaded multilevel inverters, IEEE Trans. Ind. Electron 57 (7) (2010) 2197–2206, https://doi.org/10.1109/TIE.2009.2030767.

[10] A.M. Massoud, S.J. Finney, A.J. Cruden, B.W. Williams, Three-phase, three-wire, five-level cascaded shunt active filter for power conditioning, using two different space vector modulation techniques, IEEE Trans. Power Deliv. 22 (4) (2007) 2349–2361, https://doi.org/10.1109/TPWRD.2007.905447.

[11] Y. Hoon, M.A.M. Radzi, M.K. Hassan, N.F. Mailah, Operation of three-level inverter-based shunt active power filter under nonideal grid voltage conditions with dual fundamental component extraction, IEEE Trans. Power Electron 33 (9) (2018) 7558–7570, https://doi.org/10.1109/TPEL.2017.2766268.

[12] B.P. McGrath, D.G. Holmes, Multicarrier PWM strategies for multilevel inverters, IEEE Trans. Ind. Electron 49 (4) (2002) 858–867, https://doi.org/10.1109/TIE.2002.801073.

[13] M. Angulo, P. Lezana, S. Kouro, J. Rodríguez, B. Wu, Level shifted PWM for cascaded multilevel inverters with even power distribution, Proc. PESC 2007 (2007) 2373–2378, https://doi.org/10.1109/PESC.2007.4342382.

[14] M. Xiao, Q. Xu, H. Ouyang, An improved modulation strategy combining phase shifted PWM and phase disposition PWM for cascaded H-bridge inverters, Energies 10 (9) (2017) 1327, https://doi.org/10.3390/en10091327.

[15] O.J.K. Oghorada, L. Zhang, B.A. Esan, E. Dickson, Carrier-based sinusoidal pulse-width modulation techniques for flying capacitor modular multi-level cascaded converter, Heliyon 5 (12) (2019) e03022, https://doi.org/10.1016/j.heliyon.2019.e03022.

[16] Y. Hoon, H. Ahmad, Voltage balancing for active power filter using dual-frequency multicarrier modulation with balanced H-bridge control, ePrime Adv. Electr. Eng. Electron. Energy 8 (2024) 100598, https://doi.org/10.1016/j.prime.2024.100598.

[17] S. Srimatha, B. Mallala, J. Upendar, A novel ANFIS-controlled customized UPQC device for power quality enhancement, J. Electr. Syst. Inf. Technol. 10 (1) (2023) 1–15, https://doi.org/10.1186/s43067-023-00121-1.

[18] O. Sánchez Vargas, L.G. Vela Valdés, M. Borunda, R.E. Lozoya-Ponce, J. Aguayo Alquicira, S.E. De León Aldaco, ANFIS-PSO-based optimization for THD reduction in cascaded multilevel inverter UPS systems, Electronics 13 (22) (2024) 4456, https://doi.org/10.3390/electronics13224456.

[19] S. Hou, J. Fei, Y. Chu, C. Chen, Experimental investigation of adaptive fuzzy global sliding mode control of single-phase shunt active power filters, IEEE Access 7 (2019) 64442–64449, https://doi.org/10.1109/ACCESS.2019.2917020.

[20] D. Buła, G. Jarek, J. Michalak, M. Zygmanowski, Control method of four-wire active power filter based on three-phase neutral point clamped T-type converter, Energies 14 (24) (2021) 8427, https://doi.org/10.3390/en14248427.

[21] A.B. Muljono, I.M. Ginarsa, I.M.A. Nrartha, A. Dharma, Coordination of adaptive neuro fuzzy inference system (ANFIS) and type-2 fuzzy logic system-power system stabilizer (T2FLS-PSS) to improve a large-scale power system stability, Int. J. Electr. Comput. Eng. 8 (1) (2018) 76–86, https://doi.org/10.11591/ijece.v8i1.pp76-86.

[22] S.A. Saadat, S.M. Ghamari, H. Mollaee, F. Khavari, Adaptive neuro-fuzzy inference systems (ANFIS) controller design on single-phase full-bridge inverter with a cascade fractional-order PID voltage controller, IET Power Electron 14 (11) (2021) 1960–1972, https://doi.org/10.1049/pel2.12162.

[23] J. Samanta, R. Sangno, R. Pudur, Enhancement of power quality in edge-of-grid systems: MCCF-SRF based control for dynamic load compensation, IEEE Trans. Ind. Appl. 61 (2025) 1–8, https://doi.org/10.1109/TIA.2025.

[24] G. Mühürcü, E. Köse, A. Muhurcu, A. Kuyumcu, Parameter optimization of PI controller by PSO for optimal controlling of a buck converter's output. In: Proceedings of the 2017 Int. Artif. Intell. Data Process. Symp. (IDAP), 2017. pp. 1–6, https://doi.org/10.1109/IDAP.2017.8090234.

[25] A.T. Nguyen, T. Taniguchi, L. Eciolaza, V. Campos, R. Palhares, M. Sugeno, Fuzzy control systems: past, present and future, IEEE Comput. Intell. Mag. 14 (1) (2019) 56–68, https://doi.org/10.1109/MCI.2018.2881644.

[26] A. Fitriani, A. Amirullah, K. Bhumkittipich, Power quality enhancement using single phase shunt active filter based ANFIS supplied by photovoltaic, Vokasi Unesa Bull. Eng. Technol. Appl. Sci. 2 (3) (2025) 558–580, https://doi.org/10.26740/vubeta.v2i3.39071.

[27] M.M. Tounsi, A. Allali, H. Merabet Boulouiha, M. Denaï, ANFIS control of a shunt active filter based with a five-level NPC inverter to improve power quality, Int. J. Electr. Comput. Eng. 11 (3) (2021) 1886–1893, https://doi.org/10.11591/ijece.v11i3.pp1886-1893.

[28] R. Boopathi, V. Indragandhi, Experimental investigations on photovoltaic interface neutral point clamped multilevel inverter-based shunt active power filter to enhance grid power quality, IEEE Access 12 (2024) 74482–74498, https://doi.org/10.1109/ACCESS.2024.3405533.

[29] U.K. Gupta, D. Sethi, P.K. Goswami, Adaptive TS-ANFIS neuro-fuzzy controller based single phase shunt active power filter to mitigate sensitive power quality issues in IoT devices, ePrime Adv. Electr. Eng. Electron. Energy 8 (2024) 100542, https://doi.org/10.1016/j.prime.2024.100542.

[30] A. Bressane, A.J. Da Silva Garcia, M.V. De Castro, S.D. Xerfan, G. Ruas, R.G. Negri, Fuzzy machine learning applications in environmental engineering: does the ability to deal with uncertainty really matter, Sustainability 16 (11) (2024) 4525, https://doi.org/10.3390/su16114525.

[31] O.B. Adewuyi, S. Krishnamurthy, Performance analysis for predictive voltage stability monitoring using enhanced adaptive neuro-fuzzy expert system, Mathematics 12 (19) (2024) 3008, https://doi.org/10.3390/math12193008.

[32] D. Michie, D.J. Spiegelhalter, C.C. Taylor, J. Campbell (Eds.), Machine learning, neural and statistical classification, Ellis Horwood, 1995.

[33] I.M. Ginarsa, A. Soeprijanto, M.H. Purnomo, Controlling chaos and voltage collapse using an ANFIS-based composite controller-static var compensator in power systems, Int. J. Electr. Power Energy Syst. 46 (1) (2013) 79–88, https://doi.org/10.1016/j.ijepes.2012.10.005.

[34] A. Bughneda, M. Salem, A. Richelli, D. Ishak, S. Alatai, Review of multilevel inverters for PV energy system applications, Energies 14 (6) (2021) 1585, https://doi.org/10.3390/en14061585.

[35] C.S. Han, H. Ahmad, H. Yap, Voltage balancing control for single-phase 5-level cascaded H-bridge inverter in performing harmonic mitigation. In: Proceedings of the 2024 International Conference on Green Energy, Computing and Sustainable Technology (GECOST), 2024. pp. 316–321, https://doi.org/10.1109/GECOST60902.2024.10474797.

[36] M.A.A.M. Zainuri, M.A.M. Radzi, A.C. Soh, N. Mariun, N.A. Rahim, DC-link capacitor voltage control for single-phase shunt active power filter with step size error cancellation in self-charging algorithm, IET Power Electron. 9 (2) (2016) 323–335, https://doi.org/10.1049/iet-pel.2015.0126.

[37] Y. Wang, Y. Wang, S.Z. Chen, G. Zhang, Y. Zhang, A simplified minimum DC-link voltage control strategy for shunt active power filters, Energies 11 (9) (2018) 2407, https://doi.org/10.3390/en11092407.